6th IEEE RAS/EMBS International Conference on
Biomedical Robotics and Biomechatronics (BioRob)
June 26-29, 2016. UTown, Singapore

Towards Real-Time Shape Sensing of Continuum Manipulators Utilizing Fiber Bragg Grating Sensors

Amirhossein Farvardin, *Student Member, IEEE,* Ryan J. Murphy, Robert B. Grupp, Iulian Iordachita, *Senior Member, IEEE*, and Mehran Armand, *Member, IEEE*

***Abstract*— Fiber Bragg grating (FBG) sensors are a promising tool for real-time shape reconstruction of dexterous continuum manipulators (DCM). We have recently developed a novel FBG-based shape sensor which is capable of detecting a radius of curvature of 15 mm for a 35 mm length DCM. This paper aims to further evaluate the accuracy of this shape sensor during motion of the DCM. Different experiments were performed including free bending, bending in the presence of an obstacle, and bending with a tool inserted in the lumen of the DCM. Results indicate that this sensor can track the tip position with an average error of 0.81 mm for free bending, 2.73 mm for bending with an obstacle, and 0.93 mm for bending with a tool.**

I. Introduction

Due to their capability to increase the reachable regions for the operation, dexterous manipulators (DCMs) and flexible tools have been commonly used in minimally and less-invasive surgery [1-6]. We have previously developed a cable-driven DCM designed for treatment of osteolysis (bone degradation) after hip replacement surgery (Fig. 1(a)). Utilizing the DCM, surgeons will be able to access the region behind the implant through the screw holes of the well-fixed acetabular component (Fig. 1(b)) [5]. Studies suggest the DCM could help to remove nearly the entire osteolytic lesion [7].

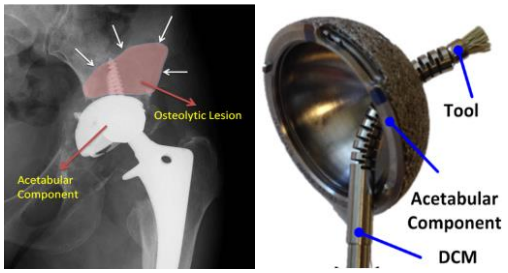

Figure 1. The (a) osteolysis and (b) DCM and tool insertion through screw hole of an implant [17, 20]

*Research supported by NIH grant R01 EB016703

Amirhossein Farvardin is with Laboratory for Computational Sensing and Robotics (LCSR) and Department of Mechanical Engineering, Johns Hopkins University, Baltimore, Maryland, USA (email: afarvar1@jhu.edu, phone: 508-615-9060)

Robert Grupp, Iulian Iordachita and Mehran Armand are with Laboratory for Computational Sensing and Robotics (LCSR), Johns Hopkins University, Baltimore, Maryland, USA (emails: Ryan.Murphy@jhuapl.edu, grupp@jhu.edu, iordachita@jhu.edu, and Mehran.Armand@jhuapl.edu)

Ryan J. Murphy and Mehran Armand are with the Research and Engineering Development Department, Johns Hopkins University Applied Physics Laboratory, Laurel, Maryland, USA

Real-time control of the DCM requires a system that can accurately track the DCM shape and estimate its tip position, even for large deflections. Previous efforts involved modeling the DCM shape from cable length measurements [6, 7] and intermittent use of 2D X-ray images for shape reconstruction [8]. Due to the limited accuracy of models from cable-length measurements in obstructed environments such as human body, and the large amount of radiation exposure from X-ray images, these approaches have not been effective for real-time control of the DCM. Other shape sensing techniques that have been considered for continuum manipulators include electromagnetic (EM) sensors and piezoelectric polymers [9]. The accuracy of EM sensors is suitable for most medical applications, but the major challenge with these sensors is their robustness in the presence of metals [10]. Piezoelectric polymers are shown to be stable and capable of large deflection shape sensing, but their mechanical hysteresis has been reported to be about 16% of the resting length which is a limitation for use in medical applications [9]. Searle, et al. applied a light intensity modulation sensing for measurement of the curvature between two rigid segments of a robot consisting of rigid and flexible segments [11]. In addition to shape tracking, different studies have looked at the algorithms that can detect potential obstacles and control the manipulator in those scenarios [12, 13].

Fiber Bragg grating (FBG) sensors are considered a viable approach for real-time shape sensing of continuum robots for various reasons including their light weight, stability, high sensitivity, and fast response. Park et al. attached FBG sensors to an MRI-compatible biopsy needle to track the needle's shape as it was inserted into tissues [14]. Roesthuis et al. used a similar technique and attached 3 arrays of 12 FBG sensors to a 172 mm long nitinol needle for 3D shape reconstruction [15]. In the case of our DCM, shape sensors are required to detect much larger deflections compared to those of needle steering. For this purpose, we recently proposed a novel FBG-based shape sensor with an ability to detect a radius of curvature of 15 mm for a 35 mm DCM with an average calibration error of 3.14% [16]. In a static environment (i.e., the manipulator was not moving), this technique was further verified in the presence of obstacles and the shape reconstruction error was evaluated [17].

Although the FBG-based shape sensor has shown reasonable accuracy in static cases, none of the previous studies have considered large deflection shape tracking in dynamic cases or with tools inserted through the lumen of the DCM. Therefore, it is important to further evaluate the accuracy and precision of the sensor during the motion of the

DCM, before utilizing the sensor's feedback in a control loop. In this paper, we evaluate the effectiveness of FBG-based shape tracking in different scenarios including free bending, and bending in the presence of an obstacle. We also examined the effects of tool insertion on shape sensing where friction is the major source of disturbance. Section II presents the basic concept of FBG-based curvature detection and the algorithm used to reconstruct the DCM's shape. Section III describes the experimental platform and the different experiments performed. Experimental results are presented in Section IV and are discussed in Section V. Section VI provides a brief conclusion.

II. Shape Sensing Approach

A. Base Concept

Estimating the manipulator shape is akin to measuring the curvature of the manipulator's centerline at any point along its length. For this purpose, we have utilized two shape sensor arrays. Each array contains 3 FBG sensors distributed 10 mm apart (Technica SA, China). The wavelength shift ($\Delta\lambda$) of each active node is given by (1) [18]:

$$\Delta\lambda = k_\varepsilon \varepsilon + k_T \Delta T \qquad (1)$$

where ε is the strain induced in the FBG sensor, ΔT is the change in temperature, k_ε is the strain coefficient, and k_T is the temperature coefficient. This relation shows that if the temperature influence is fully compensated in the system, wavelength shift and strain are proportional.

It has been shown that FBG fibers can handle strain values smaller than 0.5% before breaking [19]. To keep the strains within this limit, we have implemented a strategy fully described by Liu et al. [16]. The shape sensor array was designed with one FBG fiber and two nitinol wires bonded together. This array was inserted in the channels through the walls of the DCM and was fixed at the distal end. This array can freely move along the DCM preventing local stress concentration on the fiber. Fig. 2 shows the assembled sensor under microscope (ZEISS, Germany) at 25 times magnification.

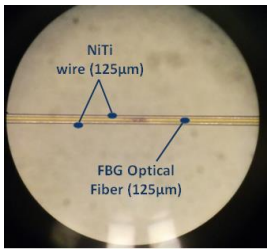

Figure 2. Configuration of the shape sensing bundle under microscope

After assembly, the linear relationship between the curvature and wavelength shift of the sensors were calculated utilizing a multi-channel calibration board with different curvature slots. This relationship is given by [17]:

$$\kappa = \frac{\Delta\lambda}{k_\varepsilon \cdot \delta} \qquad (2)$$

where κ is curvature and δ denotes the biased distance of FBG core from the neutral plane.

B. Shape Reconstruction

To reconstruct the DCM shape from discrete FBG data, we first defined a shape curve along each of the sensors by starting from the distal end where the sensors are fixed [17]. Linear interpolation estimated the curvature between sensors, while the curvature of proximal and distal regions of the DCM was assumed constant. Since FBG placement is on the outer surface of the DCM, the curves must offset toward the centerline of the DCM (Fig. 3). The tangent angle along the length of the DCM and the 2D coordinates for series of distinct points is calculated by (3) and (4) [16]:

$$\theta(s) = \int_0^s \kappa(s) ds + \theta_0 \qquad (3)$$

$$\begin{cases} \Delta x = \cos\theta(s) \cdot \Delta s \\ \Delta y = \sin\theta(s) \cdot \Delta s \end{cases} \qquad (4)$$

where θ is the tangent angle and s is the arc length.

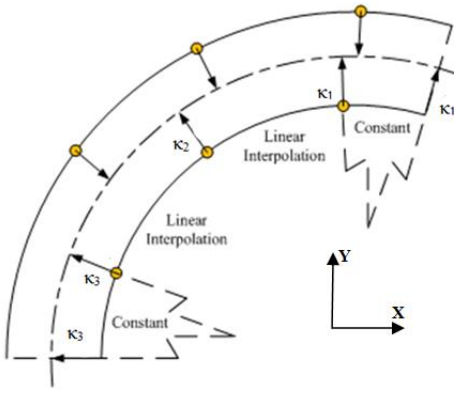

Figure 3. Arrangement of the FBG sensors inside the DCM [16]

III. Experimental Platform and Shape Tracking Cases

A. Experimental Platform

Experiments evaluated the accuracy of the shape tracking during the manipulator's motion. Fig. 4 shows the experimental platform, which included a custom actuation unit, FBG interrogator (Micron Optics, USA), and PL-B741 camera (PixelLink, USA). Three types of experiments were performed: 1) free bending (i.e., no external loads applied to the DCM), 2) bending in the presence of an obstacle, and 3) bending in the presence of a tool inside the inner-lumen. The FBG interrogator recorded the wavelengths of each FBG sensor during the experiment and also the estimated tip position based on these wavelengths. The calibrated overhead camera captured planar images of the DCM at 0.5 mm increments of cable displacement to analyze and compare to the shape sensor data as a ground truth. The DCM actuation unit utilized a 3 mm diameter, 1 mm lead ball screw assembly (Steinmeyer, Germany) to actuate both drive-cables during each bending cycle [20]. Custom C++ software controlled the DCM and collected synchronized data from the shape sensors and the camera.

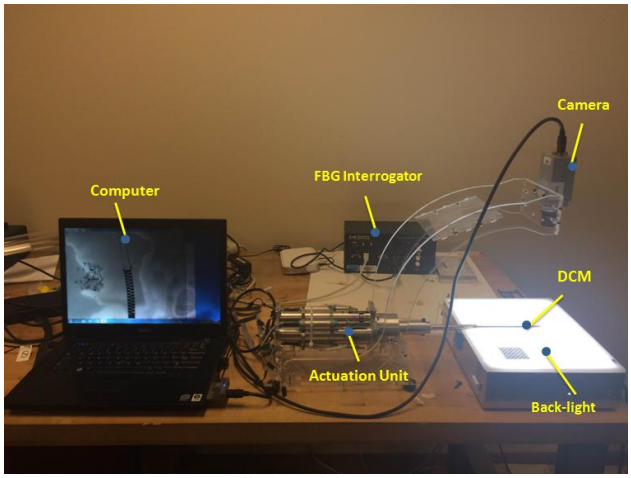

Figure 4. Overall view of the experimental setup

B. Case I: Free bending

A total of 3 free bending experiments with variable cable displacement rates (0.5 mm/s, 0.75 mm/s, and 1 mm/s) were performed. With these rates, the DCM can bend to the maximum cable displacement of 3 mm in 6, 4, and 3 seconds, respectively. Prior to each experiment, a manual calibration procedure defined the zero cable position. Zero position is the point where the cable is in tension and if a small delta is applied to the cable position, the DCM starts to bend [20]. In each experiment, the DCM was actuated for 5 bending cycles. Each cycle included free-bends to 3 mm cable displacement and return to the zero position on both bending directions. Although this manipulator is capable of larger bends, this threshold was set to avoid potential damage to the shape sensors. Fig. 5 shows the DCM configuration during a free bending test captured by the camera.

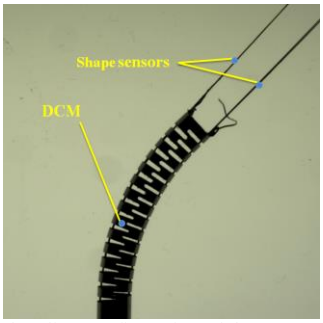

Figure 5. Free bending configuration of the DCM at 2 mm cable displacement

C. Case II: Bending with an Obstacle

Two bending experiments were carried out at 0.5 mm/s and 1.0 mm/s cable displacement rates. Similar to the free bending case, DCM actuated for 5 cycles, starting and ending at the zero position. In this case, however, maximum cable displacement was set to 2 mm. To create an obstructed environment for the DCM, a rigid path obstacle with diameter of 25 mm was fixed on one side. Fi20g. 6 shows the DCM configuration during its contact with the obstacle.

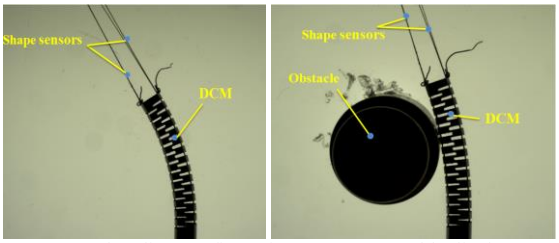

Figure 6. DCM bending configurations at 2.0 mm cable displacement in free bending (left), and bending in the presence of an obstacle

D. Case III: Bending with Tooling

A recent surgical tool developed for osteolysis treatment utilizes a flexible torque coil [21]. In this experiment, a torque coil (Asahi Int. USA, Inc.) with a 3.3 mm outer diameter was inserted in the lumen of the DCM to evaluate FBG-based shape sensing similar to the experiment for case I (Fig. 7). Each experiment ran for 5 cycles with the cable displacement rate at 0.5 mm/s and maximum cable displacement of 2 mm.

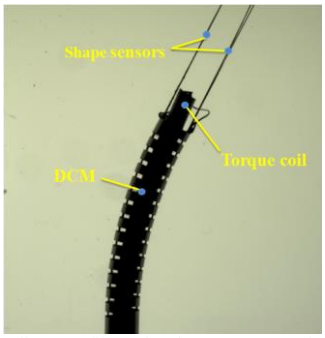

Figure 7. DCM bending configuration in a presence of a torque coil inside its lumen

E. Data Analysis

Prior to data collection, camera calibration using a square chessboard identified the intrinsic parameters. A previously validated 2D-3D registration algorithm developed by Otake et al. [8] processed each image to provide a ground truth DCM shape. This method outputs the shape curve associated with the DCM's centerline, given a planar image of the DCM. The method optimizes a normalized gradient information similarity metric between a reconstructed 2D image and the raw camera data. Registration results served as the ground truth to evaluate the tracking accuracy of the sensors. For this purpose, the timestamp of each camera image is used to associate each ground truth measurement with the appropriate FBG data. Linear interpolation of the FBG measurements is performed when an image timestamp lies between two FBG measurements. We compared the ground truth coordinates with the corresponding values measured by the shape sensors to measure error. ANOVA analysis of variance was performed to compare different experimental groups.

IV. Results

The average and standard deviation of the tip tracking errors of all experimental cases are shown in Table 1. In the free-bending case with a 0.5 mm/s cable displacement rate, mean error was 1.14 ± 0.77 mm. This value increased to

3.49 ± 1.3 mm when the cable displacement rate changed from 0.5 mm/s to 1.0 mm/s. These values correspond to 3.25% and 9.9% of the DCM's length, respectively. In the case of bending with an obstacle, the average error was 2.73 ± 0.77 mm which is 7.8% of the DCM's length. In the case of bending with a tool, the average error was 0.93 ± 0.59 mm or 2.6% of the DCM's length. ANOVA analysis of variance shows that free bending accuracy is significantly different with those of bending with an obstacle ($p > 0.99$). However, these is no significant difference ($p=0.96$) between the shape sensing accuracy with and without a tool.

Table 1. Summary of tip tracking results for all experimental groups

Case	*Cable displacement rate [mm/s]*	*Max Cable displacement [mm]*	*# of Images per cycle*	*Mean trajectory error [mm]*	*Standard deviation of error [mm]*
Free bending	**0.5**	**3.0**	**24**	**1.14**	**0.77**
	0.75	**3.0**	**24**	**0.81**	**0.99**
	1.0	**3.0**	**24**	**3.49**	**1.3**
bending with an obstacle	**0.5**	**2.0**	**16**	**2.73**	**0.77**
	1.0	**2.0**	**16**	**0.96**	**0.35**
bending with a tool	**0.5**	**2.0**	**16**	**0.93**	**0.59**

Using the extracted cordinates of the tip position from the images and sensor data, planar trajectories of the tip position were plotted for 3 cases of free bending (Fig. 8), bending with an obstacle (Fig. 9), and bending with a tool (Fig. 10).

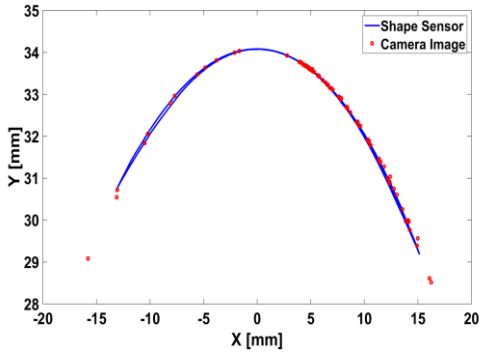

Figure 8. Comparison of shape sensing trajectory with the trajectory extracted from 120 images-free bending

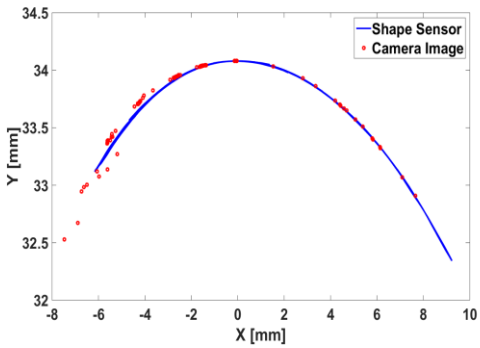

Figure 9. Comparison of shape sensing trajectory with the trajectory extracted from 80 images-bending with an obstacle (Note: In this experiment, the obstacle was fixed on the left side of the DCM (Fig. 6))

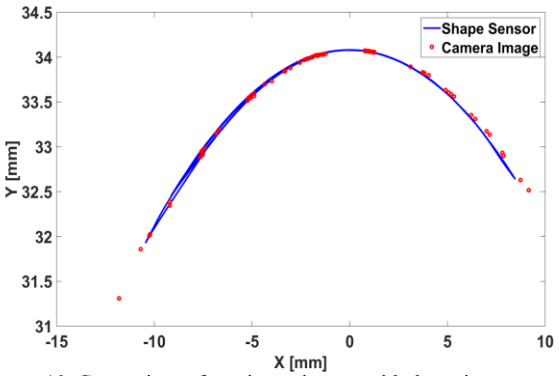

Figure 10. Comparison of sensing trajectory with the trajectory extracted from 80 images for bending with a tool

To find the exact sources of error, we have considered a free bending experiment with the cable displacement rate of 0.75 mm/s and examined the tip position on the x-axis (Fig. 11) and y-axis (Fig. 12) separately. In this case, tip tracking had an error of 0.76 ± 0.92 mm in the x-direction and a mean error of 0.25 ± 0.36 mm in the y-direction.

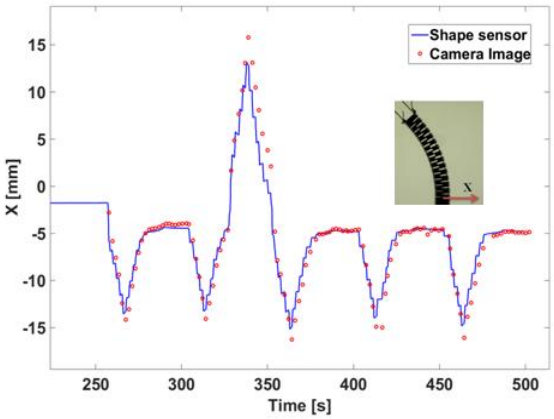

Figure 11. Tip position on the x-axis- free bending case at 0.75 mm/s cable displacement rate

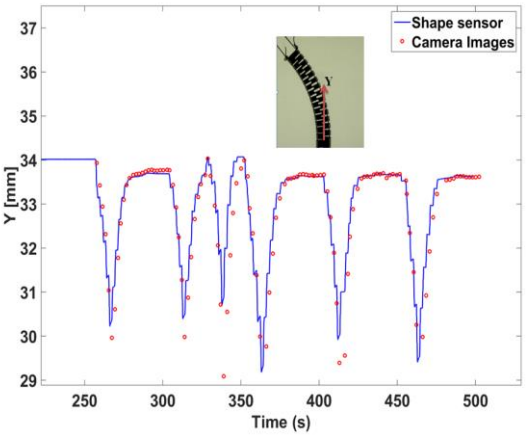

Figure 12. Tip position on the y-axis- free bending case at 0.75 mm/s cable displacement rate

V. Discussion

A. Tracking Accuracy for Free Bending

It was previously shown by Liu et al. that FBG sensors are capable of detecting the DCM's tip position with an average error of 1.1% of the DCM's length in a static case [17]. In contrast to the experiment performed by Liu et al., the experiments performed as a part of this work, considered a dynamic case when the DCM is undergoing continuous bends. It showed, through 120 captured images during the free bending test (rate = 0.75 mm/s), that if the DCM is moving, the average error increases to 2.31% of the DCM's length. In each of the bending cycles, the maximum error occurred at the maximum cable displacement. Due to a higher range of motion in the direction of x-axis (Fig. 3), tip tracking experienced a larger error in this direction, compared to errors of the y-axis. Considering the immediate application of this DCM for osteolysis treatment, the 2.31% error will not jeopardize the safety since there are no critical tissues or organs in the operating space of the DCM. We have also seen that if the DCM bends twice as fast (1 mm/s), the error increases to about 10% of the DCM's length. Therefore, it is important to identify obstacles and if we want to consider the feedback from FBG sensors in the control loop. We do not, however, foresee a requirement for fast motion of DCM when debriding osteolytic defects behind the acetabular implant.

B. Bending with an Obstacle

One of the main characteristics of the operating space in treatment of osteolysis is the presence of obstacles. Therefore, it is important to evaluate shape sensing capabilities of the FBG-sensors in those environments. When the DCM is in contact with an obstacle (Fig. 8), it begins to deform and the linear interpolation of the curvature between sensing nodes may not be accurate. For this reason, the increased error of 7.8% of the DCM's length was expected. One way to avoid this error is to increase the number of sensing nodes on each sensor. However, given the limited range of the interrogator, adding more sensing nodes is challenging. Further studies are required to evaluate shape sensing with an increased number of sensing nodes, as well as the optimization algorithms to find the optimum location of the FBG sensing nodes along the DCM. To avoid potential damages to the DCM and FBG-sensors maximum cable displacement was reduced to 2 mm in these experiments.

C. Bending with a Tool

A major advantage of the osteolysis DCM is the 6 mm inner-lumen. In the treatment procedure, surgeons can use the DCM to introduce flexible tools to the operating area. The tools, however, may alter the trajectory of the DCM by changing the system stiffness [22]. In this case, we evaluated shape sensing accuracy when a torque coil was inserted inside the DCM lumen. Results indicate that there is no significant difference ($p=0.96$) between the shape sensing accuracy with and without a tool. Due to increased stiffness of the DCM in the presence of a tool, these experiments were also conducted with maximum cable displacement of 2 mm.

D. Limitations

We used camera images along with the 2D/3D registration algorithm of Otake et al. as the ground truth. However, the mean error of 0.4 mm associated with this technique may also affect the analysis [8]. In addition, lower frequency of images compare to FBG data collection may introduce an error while considering the experimental cases with faster cable displacement rate. Although all experiments were performed at the room temperature, small temperature changes may introduce an error in our calculations. In addition, accuracy of the shape sensors is dependent on the reference wavelengths which are defined as the wavelengths of the sensors at zero position. Potential changes to the DCM configuration during the initialization, is another source of error for these experiments.

VI. Conclusion

This paper evaluates the capability of our shape sensing technique for a 35 mm length DCM in 3 dynamic cases. Results have shown that FBG sensors can track the tip position with an average error of 0.81 mm. It was also shown that there's no significant difference between the accuracy of free bending with those of bending with a tool ($p=0.96$). However, we have observed a significant increase of mean error in the presence of an obstacle ($p>0.99$).

Findings of this paper can create means for accurate real-time control of the DCM in minimally and less-invasive surgical procedures. Future works will involve optimization algorithms to define the number and locations of sensing nodes for accurate shape sensing in obstructed environments. In the future, we will also extend this work to shape sensing of 3D continuum manipulators.

Acknowledgment

We would like to thank Michael Pozin for helping with experiments and Dr. Yoshito Otake for providing the 2D-3D image registration software.

References

[1] N. Sarli, T. Marien, S.D. Herrell and N. Simaan, "'Characterization of resection dexterity in transurethral resection of bladder tumor: A kinematic study," In *Robotics and Automation (ICRA), 2015 IEEE International Conference on,* May 2015, pp. 5324-5329.

[2] R.J. Webster III, J.M. Romano and N.J. Cowan, "'Mechanics of precurved-tube continuum robots," *Robotics, IEEE Transactions on*, vol. 25, no. 1, pp. 67-78, 2009.

[3] D.B. Camarillo, C.F. Milne, C.R. Carlson, M.R. Zinn and J.K. Salisbury, "'Mechanics modeling of tendon-driven continuum manipulators," *Robotics, IEEE Transactions on*, vol. 24, no. 6, pp. 1262-1273, 2008.

[4] N. Simaan, R. Taylor and P. Flint, "'High dexterity snake-like robotic slaves for minimally invasive telesurgery of the upper airway," In *Medical Image Computing and Computer-Assisted Intervention–* MICCAI 2004, Sep 2004, pp. 17-24.

[5] M.D. Kutzer, S.M. Segreti, C.Y. Brown, M. Armand, R.H. Taylor and S.C. Mears, "'Design of a new cable-driven manipulator with a large open lumen: Preliminary applications in the minimally-invasive removal of osteolysis," *In Robotics and Automation (ICRA), 2011 IEEE International Conference on*, May 2011, pp. 2913-2920.

[6] S.M. Segreti, M.D. Kutzer, R.J. Murphy and M. Armand, "'Cable length estimation for a compliant surgical manipulator," In *Robotics and Automation (ICRA), 2012 IEEE International Conference on*, May 2012 pp. 701-708.

[7] R.J. Murphy, M.D. Kutzer, S.M. Segreti, B.C. Lucas and M. Armand, "'Design and kinematic characterization of a surgical manipulator with a focus on treating osteolysis," *Robotica*, vol. 32, no. 06, pp. 835-850, 2014.

[8] Y. Otake, RJ. Murphy, M. Kutzer, R. Taylor and A. Mehran, "'Piecewise-rigied 2D-3D registration for pose estimation of snake-like manipulator using an intraoperative x-ray projection," *In SPIE Medical Imaging*, Feb 2014, pp. 90360Q-90360Q-6.

[9] M. Cianchetti, F. Renda, A. Licofonte and C. Laschi, "'Sensorization of continuum soft robots for reconstructing their spatial configuration," *Biomedical Robotics and Biomechatronics (BioRob)*, June 2012, pp. 634-639.

[10] A.M. Franz, T. Haidegger, W. Birkfellner, K. Cleary, T.M. Peters and L. Maier-Hein, "Electromagnetic Tracking in Medicine—A Review of Technology, Validation, and Applications," *Medical Imaging, IEEE Transactions on*, vol. 33, no. 8, pp. 1702-1725, 2014

[11] T.C. Searle, K. Althoefer, L. Senevirante, and H. Liu, "An optical curvature sensor for flexible manipulators," *Robotics and Automation (ICRA), 2013 IEEE International Conference on*, May 2013, pp. 4415-4420.

[12] A. Bajo and N. Simaan, "'Kinematics-based detection and localization of contacts along f continuum robots," *Ro, botics, IEEE Transactions on*, vol. 28, no. 2, pp. 291-302, 2012.

[13] J. Li and J. Xiao, "'Task-constrained continuum manipulation in cluttered space," *Robotics and Automation (ICRA), 2014 IEEE International Conference on*, May 2014, pp. 2183-2188.

[14] Y. Park, S. Elayaperumal, B. Daniel, S.C. Ryu, M. Shin, J. Savall, R.J. Black, B. Moslehi and M.R. Cutkosky, "'Real-time estimation of 3-D needle shape and deflection for MRI-guided interventions," *Mechatronics, IEEE/ASME Transactions on*, vol. 15, no. 6, pp. 906-915, 2010.

[15] R.J. Roesthuis, M. Kemp, van den Dobbelsteen, John J and S. Misra, "'Three-dimensional needle shape reconstruction using an array of fiber bragg grating sensors," *Mechatronics, IEEE/ASME Transactions on*, vol. 19, no. 4, pp. 1115-1126, 2014

[16] H. Liu, A. Farvardin, S.A. Pedram, I. Iordachita, R.H. Taylor and M. Armand, "'Large deflection shape sensing of a continuum manipulator for minimally-invasive surgery," *In Robotics and Automation (ICRA), 2015 IEEE International Conference on*, May 2015, pp 201-206.

[17] H. Liu, A. Farvardin, R. Grupp, R. Murphy, R. Taylor, I. Iordachita and M. Armand, "'Shape tracking of a dexterous continuum manipulator utilizing two large deflection shape sensors," *In Sensors Journal, IEEE,* vol. 15, no. 3, pp. 5494-5503, 2015.

[18] X. He, J. Handa, P. Gehlbach, R. Taylor and I. Iordachita, "'A submillimetric 3-dof force sensing instrument with integrated fiber bragg grating for retinal microsurgery," *Biomedical Engineering, IEEE Transactions on*, vol. 61, no. 2, pp. 522-534, 2014.

[19] F. Araújo, L. Ferreira, J. Santos and F. Farahi, "'Temperature and strain insensitive bending measurements with D-type fibre Bragg gratings," *Measurement Science and Technology*, vol. 12, no. 7, pp. 829, 2001.

[20] R.J. Murphy, Y. Otake, R.H. Taylor and M. Armand, "'Predicting kinematic configuration from string length for a snake-like manipulator not exhibiting constant curvature bending,", In *Intelligent Robots and Systems (IROS) 2014, IEEE/RSJ International Conference on*, Sep 2014, pp. 3515-3521.

[21] F. Alambeigi, S. Sefati, R.J. Murphy, I. Iordachita, M. Armand, "'Design and Characterization of a Debriding Tool in Robot-Assosted Treatment of Osteolysis," *In Robotics and Automation (ICRA), 2016 IEEE International Conference on,* May 2016 [Accepted]

[22] R.J. Murphy, Y. Otake, K.C. Wolfe, R.H. Taylor and M. Armand, "'Effects of tools inserted through snake-like surgical manipulators," In *Engineering in Medicine and Biology Society (EMBC),* Aug 2014, pp. 6854-6858.